Applied Surface Science 582 (2022) 152356

Contents lists available at ScienceDirect

Applied Surface Science

journal homepage: www.elsevier.com/locate/apsusc

Full length article

Ab-initio-driven prediction of puckered penta-like PdPSeX (X=O, S, Te) Janus monolayers: Study on the electronic, optical, mechanical and photocatalytic properties

A. Bafekry [a,b,*], M. Faraji [c], Mohamed M. Fadlallah [d], H.R. Jappor [e], N.N. Hieu [f,g], M. Ghergherehchi [h], D. Gogova [i]

[a] Department of Physics, University of Guilan, Rasht 41335-1914, Iran
[b] Department of Physics, Rasht Branch, Islamic Azad University, Rasht Iran
[c] Micro and Nanotechnology Graduate Program, TOBB University of Economics and Technology, Sogutozu Caddesi No 43 Sogutozu, 06560, Ankara, Turkey
[d] Department of Physics, Faculty of Science, Benha University, 13518 Benha, Egypt
[e] Department of Physics, College of Education for Pure Sciences, University of Babylon, Hilla, Iraq
[f] Institute of Research and Development, Duy Tan University, Da Nang 550000, Viet Nam
[g] Faculty of Natural Sciences, Duy Tan University, Da Nang 550000, Viet Nam
[h] College of Electronic and Electrical Engineering, Sungkyunkwan University, Suwon, Republic of Korea
[i] Department of Physics, Chemistry and Biology, Linkoping University, 58183 Linkoping, Sweden

ARTICLE INFO

Keywords:
2D materials
Puckered penta-like structure
PdPSeX (X=O, S, Te)
Janus monolayers
Electro-optical and mechanical properties
Photocatalytic properties
Ab-initio-driven prediction

ABSTRACT

A systematic investigation of the structural, mechanical, electronic, and optical properties of puckered penta-like PdPSeX (X=O, S and Te) Janus monolayers has been performed by means of the plane wave density functional theory. It is confirmed that the pentagonal PdPSeX monolayers are dynamically and mechanical stable by means of analysis of their phonon dispersion curves and the Born condition under harmonic approximation, respectively. The PdPSeX Janus monolayers are disclosed as brittle two-dimensional materials (2DMs). The PBE (HSE06)-based calculations exhibit they are indirect semiconductors with bandgap values of 0.65 (1.44) eV, 1.20 (2.02) eV, and 0.98 (1.70) eV for PbPSeO, PbPSeS, and PbPSeTe monolayer, sequentially. The computational results demonstrate the PdPSeTe monolayer as the best suited candidate for visible light absorption and photocatalytic water splitting within the considered pentagonal PdPSeX monolayers. Our ab-initio-based outcomes provide an insight into the fundamental properties of the penta-like PdPSeX Janus structures and surely would motivate further experimental and theoretical studies to reveal the full application potential of this new type of 2DMs.

1. Introduction

Two-dimensional (2D) transition metal dichalcogenides (TMDC) have appeared as a modern family of atomically flat materials with potential applications in optoelectronics and nanoelectronics [1–6]. Design and development of novel TMDC nanomaterials with better performance in terms of certain implementations is a hot topic nowadays. Among these TMDC, the 2D palladium-based chalcogenides materials (PdS_2 and $PdSe_2$) possessing layered structures, have received growing attention recently [7–11]. Though the hexagonal structure is dominant in 2D materials, resulting in atomically flat surfaces, the $PdSe_2$ can crystallize in several polymorphs. For example, at ambient conditions, $PdSe_2$ crystallizes in orthorhombic structure belonging to the Pbca space group [12], but under pressure the orthorhombic structure can be transformed into the cubic one [13]. Different results have been demonstrated, i.e., that $PdSe_2$ can be grown with a monoclinic [14] and a hexagonal structure with the space group P-3M1 [15]. Recently, a stable noble-metal dichalcogenide multilayer – the 2D pentagonal $PdSe_2$ – has been successfully synthesized from bulk $PdSe_2$ [16] and its promising properties for utilization in spintronics, optoelectronics, and nanoscale devices have been manifested [17,18]. Interestingly, as a result of the system structure and surface arrangement, the pentagonal 2D materials with low symmetry and a puckered structure can potentially display unique chemical and physical properties, including high stability and excellent electron mobility [19,20], opening up new opportunities for the forthcoming optoelectronic and nanoelectronic devices. Surprisingly, puckering in the pentagonal structure has

* Corresponding author.
E-mail address: bafekry.asad@gmail.com (A. Bafekry).

https://doi.org/10.1016/j.apsusc.2021.152356
Received 15 October 2021; Received in revised form 18 December 2021; Accepted 26 December 2021
Available online 10 January 2022

been discovered empirically and has been foreseen theoretically in other 2D materials such as PdS_2 [21], Al_2N [22], pentagraphene [23], penta-silicene [24], SiC_2 [25], B_2C [26], BP_5 [27], and As_2C [28].

However, according to some investigations, ternary 2D PdPSe exhibit crystal structures significantly different from that of the free-standing $PdSe_2$ monolayer [29]. More precisely, PdPS and PdPSe 2D materials appear in a crinkled shape with a pentagonal lattice, and can also crystallize into orthorhombic structures [30]. Although, studies on the properties of bulk crystalline chalcogenide PdPSe have earned a lot of interest in recent years [31–34], investigations related to the properties in the 2D limit are only getting started. Based on the first-principles calculations, Jing et al. [35] confirmed that 2D PdPS and PdPSe monolayers are semiconductors with high carrier mobilities and energy gaps of 2.12 eV and 1.95 eV, respectively. Additionally, these monolayers are kinetically and thermally stable and PdPSe and PdPS monolayers can be obtained by exfoliation from bulk crystals with low cleavage energy. In addition, it has also been confirmed that the PdPS monolayer is flexible and has a potential for a water splitting catalyst as well as for a light absorber.

Very recently, Li et al. [36] have synthesized a novel 2D penta-PdPSe with a low-level symmetry shape. The substantial intrinsic anisotropic conductivity of the new PdPSe provides diverse opto-electronic properties. Furthermore, it has been underscored the 2D penta-PdPSe exhibits a noteworthy photo responsiveness and possesses a good electronic mobility. Bafekry et al. [37] investigated the structural, mechanical, electronic, optical and thermoelectric properties of PdPSe monolayer via density functional theory calculations. These observations lead to the conclusion that 2D penta-PdPSe could be utilized in development of anisotropic devices. Janus nanostructures arrangement provides a unique approach to nanoscale 2D material design. Owing to the unusual characteristics that distinct them from ordinary 2D materials, the Janus materials are presently gaining attention. A considerable number of Janus single-layers has been experimentally fabricated or computationally suggested, including but not limited to Janus TMDC [38], MoSeTe [39], WSSe [40], BiTeCl, BiTeBr [41], Ga_2SSe, Ga_2STe, Ga_2SeTe [42], Bi_2X_3 (X=S, Se, Te) [43], FeX (X=S, Se, Te) [44], AlSb and InSb [45], PtSSe [46], $FeTe_2$ [47], MoSSe [48] and Sb_2S_3 and Sb_2Se_3 [49].

Inspired by a recent publication on 2D penta-PdPSe nanosheets with interesting properties of the Janus monolayer, we propose new 2D Janus pentagonal PdPSeX (X=O, S, Te) structures. Moreover, we thoroughly investigate their optical, electronic, structural, and mechanical properties employing the first-principles calculations. To the best of our knowledge 2D Janus PdPSeO, PdPSeO, and PdPSeO monolayers have not been explored theoretically or experimentally so far. Our computations confirm these Janus monolayers are kinetically and thermodynamically stable and last but not least exhibit semiconductor properties. The findings lead us to conclude that 2D penta-PdPSeX monolayers (X=O, S and Te) could become a feasible alternative to the existing already 2DMs in nanoelectronic and optoelectronic applications.

2. Method

We have taken advantage of the density functional theory as implemented in the Vienna *ab-initio* simulation package (VASP) [50,51] to calculate the electronic structure of the nanosheets. The plane-wave basis projector augmented wave (PAW) method was used with the generalized gradient approximation of Perdew–Burke–Ernzerhof (PBE) [52,53]. The Heyd–Scuseria–Ernzerhof (HSE06) [54] functional, with a screening parameter of 0.2 $Å^{-1}$ and an exchange mixing coefficient of 25%, has been employed to obtain more accurate values of the bandgaps. The kinetic energy cut-off was taken to be 500 eV for the plane-wave expansion, and the energy of the system was converged to below 10^{-5} eV. For atomic relaxation, the Hellmann–Feynman forces were converged to below 0.05 eV/Å. A 21 × 21 × 1 Γ-point centered Monkhorst–Pack [55] *k*-point grid was employed for the unit cells. A 20 Å vacuum space along the c-direction was used to avoid any interactions in the vertical monolayers. The charge transfer was calculated using the Bader method [56]. The phonon dispersion curves were obtained using the small displacement technique as employed in the PHONOPY code [57].

3. PdPSe monolayer

The atomic lattice of the penta-like PdPSe monolayer is shown in Figs. S1 (a) of the Supplementary information. Notice, the PdPSe monolayer has a pentagonal lattice belonging to the *Pbca* (60) space group and the calculated lattice parameters are: a = 5.86 Å and b 5.79 Å. The computed bond lengths are d_1 = 2.85 Å, d_2 = 2.48 Å, d_3 = 2.31 Å and d_4 = 2.20 Å. Furthermore, the bond angles are calculated to be θ_2 = 114.86°, θ_2 = 103.83° and θ_3 = 112.19°. The thickness of the penta-like PdPSe monolayer is determined to be 1.46 Å. All structural parameters obtained are summarized in Table 1. Using the charge transfer analysis, we have calculated that the Se atoms gain 0.18 e from the neighbor Pd and P atoms, while the cohesive energy is determined to be −3.96 eV/atom. The phonon band calculation results are illustrated in Fig. S1 (b). Obviously, the phonon dispersion is free from any imaginary frequency, uncovering the dynamical stability of the PdPSe monolayer. The phonon spectrum represents an in-plane transverse (TA) and a longitudinal (LA) acoustic mode, with a linear dispersion, and an out-of-plane flexure mode (ZA) with a quadratic dispersion in the long wavelength limit. From the electronic structure, depicted in Fig. S1(c), we discover the PdPSe Janus monolayer is a semiconductor with a band gap value of 1.26 eV and 2.07 eV within the PBE and HSE06, respectively. The valance band maximum (VBM) is located at the Γ-point, while the conduction band minimum (CBM) is located at the S-point. Apparently, the VBM and the CBM are almost isotropic around the Γ-point. The projected density of states (PDOS) of the PdPSe monolayer is exhibited in Fig. S1(d). Notice that, the VBMs are mainly composed of the Pd-$d_{z^2} - d_{xy} - d_{x^2-y^2}$, P-$s, p_x$ and Se-$p_{x,z}$ orbitals states, while the CBMs originate from the $d_{xz,yz}$, $p_{x,z}$ and $p_{x,y,z}$ of Pd, P and Se atoms of the PdPSe, respectively.

4. Janus PdPSeX monolayers

4.1. Structural properties

A top and a side view of the crystalline atomic structure of PdPSeX (X=O, S, Te) Janus monolayers with a pentagonal structure (top view) are revealed in Fig. 1. Obviously, the unit cell contains 12 atoms, including four Pd, four P, two Se, and two X atoms. In each unit cell, the Pd atoms are covalently bonded to two Se and two X atoms, located in the top and bottom planes. At the ground state, the lattice constants a (b) of the Janus PdPSeX monolayers are found out to vary from 5.57 (5.47) to 6.00 Å(5.88 Å). The lattice constant a is slightly larger than the lattice constant b. Both a and b lattice constants of the Janus PdPSeX monolayers increase as the element X changes from O to Te. This is due to the increase in the atomic radius of the element X, which leads to the increase of the P–X and Pd–X bond lengths and the lattice constants are proportional to these bond lengths. Notably, the P–P and P–Pd bond lengths are almost same in the three Janus PdPSeX monolayers considered. The evaluated structural parameters of all Janus PdPSeX structures are listed in Table 1. To examine the stability of the structures considered, first we evaluate the cohesive energy per atom, given by the following equation:

$$E_{coh} = \frac{E_{tot} - 4E_{Pd} - 4E_P - 2E_{Se} - 2E_X}{12}, \quad (1)$$

where E_{tot} is the total energy of the Janus PdPSeX monolayer; E_{Pd}, E_P, E_{Se}, and E_X stands for the energy of the isolated Pb, P, Se, and X atoms, respectively. The results obtained for the cohesive energy E_{coh} of the Janus monolayers are also presented in Table 1. Namely, the cohesive energy values of the Janus PdPSeO, PdPSeS, and PdPSeTe monolayers

Table 1
Structural, electronic and mechanical parameters of PdPSeX (X=O, S, Te) Janus monolayers, illustrated in Fig. 1, including: lattice constants a, b; bond lengths between atoms ($d_{1,2,3,4}$), bond angles between atoms ($\theta_{1,2,3}$), thickness (Δh); cohesive energy per atom, (E_{coh}); charge transfer ΔQ; work function Φ; band gap E_g with PBE (HSE06); shear modulus (S); Young's modulus (Y); and Poisson's ratio (ν), respectively.

Sys.	a, b (Å)	$d_{1,2,3,4}$ (Å)	$\theta_{1,2,3}$ (°)	Δh (Å)	E_{coh} (eV/atom)	ΔQ (e)	Φ (eV)	E_g (eV)	S (GPa)	Y (GPa)	ν
PdPSe	5.86,5.79	2.85,2.48,2.31,2.20	114.86,103.83,112.19	4.42	−3.96	−0.18	5.90	1.40 (2.07)	15.36	37.19	0.21
PdPSeO	5.57,5.47	1.58,2.25,2.28,2.22	120.29,114.38,107.04	4.18	−4.67	−1.28	5.16	0.65 (1.44)	12.11	28.65	0.18
PdPSeS	5.77,5.71	2.12,2.37,2.31,2.21	107.16,117.57,110.28	4.33	−4.17	−0.45	5.40	1.20 (2.02)	14.91	36.10	0.21
PdPSeTe	6.00,5.88	2.49,2.62,2.30,2.19	99.29,110.75,114.00	4.54	−3.82	+0.16	5.18	0.98 (1.70)	14.04	33.73	0.20

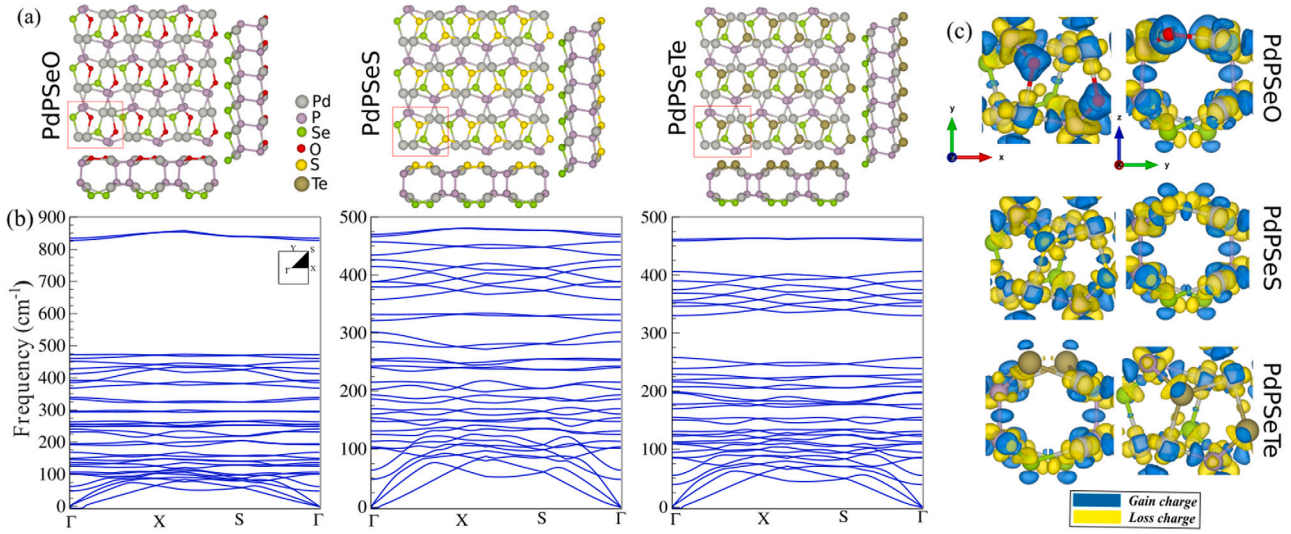

Fig. 1. Atomic structure (a), phonon band dispersion (b), and difference charge density (c) of PdPSeX (X=O, S, Te) Janus monolayers. The primitive unit cell is indicated by a red rectangular. For the difference charge density, the blue and yellow regions represent the charge accumulation and depletion, respectively.

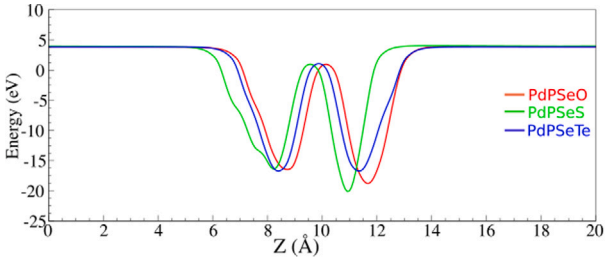

Fig. 2. Potential average of the PdPSeX (X=O, S, Te) Janus monolayers.

are evaluated to be −4.67, −4.17, and −3.82 eV/atom, accordingly. Notably, the cohesive energy values of all three Janus monolayers considered are negative, implying that their structures are energetically favorable. More importantly, we have calculated the phonon spectra of the Janus monolayers to evaluate their dynamical stability. In general, the dynamical stability of materials can be confirmed if there are no soft modes in their phonon dispersion curves. The calculated phonon spectra of the investigated monolayers are illustrated in Fig. 1(b). It is found out that all three Janus PdPSeX monolayers are dynamically stable. It should be noted that the evaluated phonon spectra have small negative frequencies near the Γ-point, which might be related to the accuracy of the numerical calculations due to the limitation in size of the supercell. Meanwhile, this does not affect the dynamical stability of the 2D materials. The difference in charge density ($\Delta\rho$) is defined as:

$$\Delta\rho = \rho_{tot} - \rho_{Pd} - \rho_P - \rho_{Se} - \rho_X, \quad (2)$$

where ρ_{tot}, ρ_{Pd}, ρ_X and ρ_P indicate the charge densities of PdPSeX and isolated Pd, P, Se and X atoms, respectively. The difference charge density is displayed in Fig. 1(c), where the blue and yellow regions represent the charge accumulation and depletion, accordingly. It is found out that the charge-depleted regions surround the P atoms in all structures. Our results show that the P atom losses approximately 0.65e (in the case of the PdPSeO Janus monolayer), 0.3e (in PdPSeS) and 0.1e (in PdPSeTe). From the difference charge densities of PdPSeO and PdPSeS, we detect that the negatively charged O and S atoms are surrounded by positively charged adjacent atoms. Notice, each O and S atom gains about 1.28e and 0.45e from the adjacent atoms in PdPSeO and PdPSeS, respectively, while in the case of PdPSeTe, the charge transfer is from the Te and it loses 0.16 e. As can be expected the charge redistribution is strongly dependent on the atomic electronegativity. The magnitudes of the charge transfer values are also included in Table 1.

In Fig. 2, we present the calculated planar average electrostatic potential of the Janus PdPSeX monolayers, which allows to evaluating their work function values. The work function is an important parameter, which enables to estimate the ability of the electrons to escape from the material's surface. Based on the electrostatic potential calculations, we can estimate the work function Φ via the Fermi E_F and vacuum E_{vac} levels as follows: $\Phi = E_{vac} - E_F$. Thus, the work function values of PdPSeO, PbPSeS, and PbPSeTe monolayers are calculated to be 5.16, 5.40, and 5.18 eV, respectively. Next, we discuss the mechanical stability and related properties of the PdPSeX sheets. The harmonic approximation is employed to calculate the linear elastic constants. The elastic parameters verify the Born conditions [58], which indicates that all PdPSeX sheets are mechanically stable. The shear moduli (S) of PdPSeO, PdPSeS and PdPSeTe monolayers are determined as 12.1 GPa, 14.9 GPa and 14.1 GPa, accordingly. The Young's moduli (Y) of PdPSeO, PdPSeS and PdPSeTe monolayers are 28.7 GPa, 36.1 GPa, and 33.7 GPa, correspondingly. The Poisson's ratio values, given in Table 1, are less than 0.33, thus, demonstrating that PdPSeX monolayers are brittle structures.

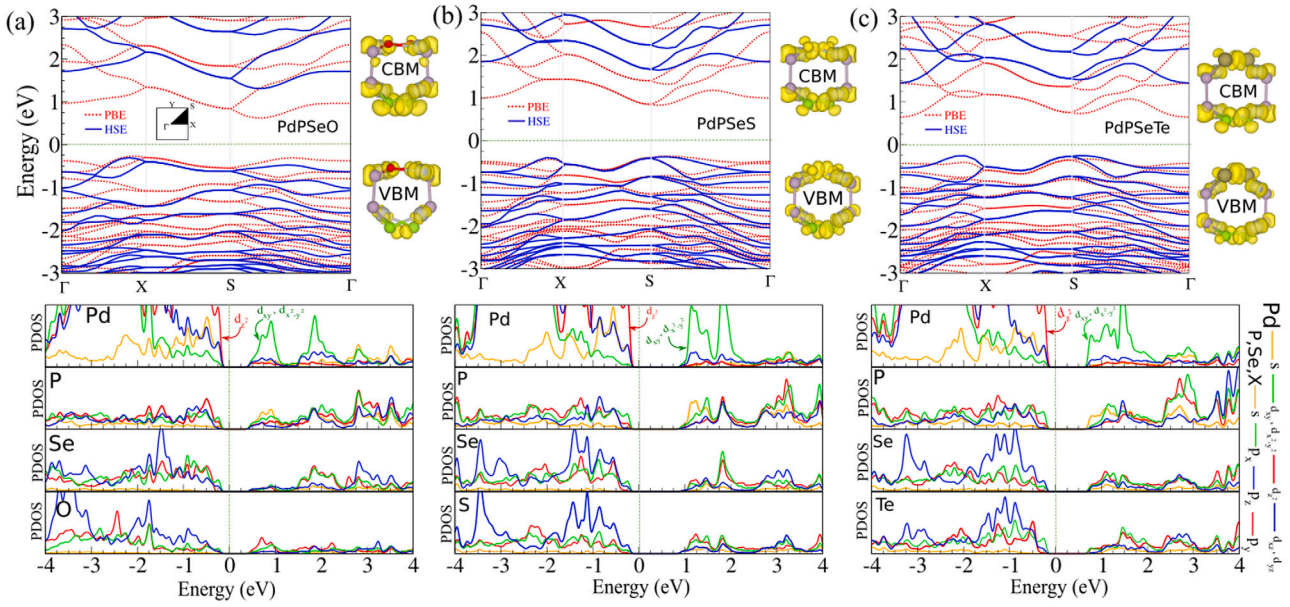

Fig. 3. (a) Electronic band structures using PBE and HSE06 with corresponding (b) DOS and PDOS of PdPSeX (X=O, S, Te) Janus monolayers (employing PBE). Zero of energy is set at the Fermi energy level. The charge density of VBM and CBM indicated as right panel of the band structure.

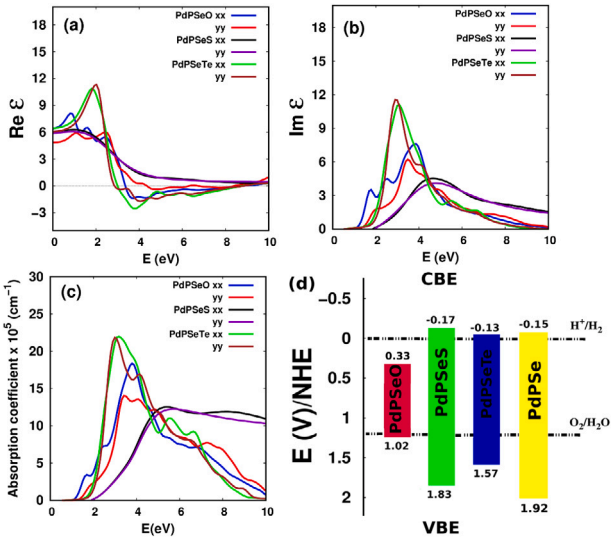

Fig. 4. Real (a) and imaginary parts (b) of the dielectric functions, and optical absorption spectra (c) as a function of the photon energy of PdPSeX (X=O, S, Te) monolayers estimated by the RPA+HSE06 approaches, and (d) band alignments of PdPSeX (X=O, S, Te) monolayers for photocatalytic water splitting and carbon dioxide reduction as compared to the PdPSe monolayer. The band edges are given with respect to the NHE potential (in Volts).

4.2. Electronic properties

Furthermore, we investigate the electronic properties of the Janus PdPSeX sheets. The calculated band structures and the corresponding partial densities of states (PDOS) of the three PdPSeX monolayers are illustrated in Fig. 3. It is found out that the Janus PdPSeO and PdPSeTe monolayers are indirect bandgap semiconductors, while the PdPSeS monolayer is a direct bandgap one. The bandgap values of PdPSeO, PdPSeS, and PdPSeTe are calculated to be 0.65 eV, 1.20 eV, and 0.98 eV at the PBE level, respectively. The bandgap values of PdPSeO, PdPSeS, and PdPSeTe decrease with approximately 30 meV, 20 meV, and 30 meV, accordingly, when a spin–orbit coupling (SOC) is considered. Moreover, we discover a band splitting of about 30 meV in the valence and conduction bands, see Figs. S2(a–c) (Supplementary information). Focusing on the band structures, one can see that the PdPSeS and PdPSeTe Janus monolayers have rather similar band structures. The VBM and CBM of the PdPSeO are located at the Γ-X path and S-Γ path, accordingly. In the case of PdPSeS they are located at the S-point, while for PdPSeTe the VBM and CBM are placed at the S-Γ path and Γ-point. The charge densities of the CBM and VBM are also indicated in Fig. 3(a). It is well-known the PBE method underestimates the bandgap values of insulators and semiconductors. However, this problem can be solved by using a hybrid functional, such as the HSE06 one. Our calculations demonstrate that the band structures estimated by the HSE06 and PBE method have almost same profiles. The most significant difference is that the bandgap value, calculated by the HSE06 hybrid functional, is much larger than the one computed by the PBE approach. Our HSE06 functional-based computational results demonstrate that all PdPSeX monolayers are indirect semiconductors with bandgap values of 1.32, 2.01 and 1.70 eV for PbPSeO, PbPSeS, and PbPSeTe, respectively. The calculated band structures of the Janus monolayers at the HES06 level are also illustrated in Fig. 3. The corresponding bandgap values are summarized in Table 1. To evaluate the contributions of orbitals of atoms to the formation of the electronic bands, we have computed the PDOS of all three Janus structures. The results are depicted in Fig. 4(b). Obviously, the electronic bands, both valence and conduction, are mainly contributed by the orbitals of the Pd atoms. Besides, the p_z orbitals have a large contribution to the valence band too. Focusing on the CBM and VBM, it is evident that the VBM of the Janus monolayers is mainly contributed by the Pd-d_{x^2} orbitals, while the $d_{xy^2}, d_{x^2+y^2}$ orbitals of the Pd atoms have a significant contribution to the CBM.

4.3. Optical properties and band alignment

Turning to the optical properties of the PdPSeX monolayers (Figs. 4(a–c)), the real and imaginary components of the dielectric function are calculated by means of the random phase approximation (RPA) method over the HSE06. The interaction between the incident electromagnetic field and the PdPSeX monolayers can be described by the dielectric function, which depends on the band structure of the monolayer. The Kramers–Kronig equations are used to evaluate the real component from the imaginary component of the dielectric function.

The real part of the dielectric function at zero energy is the static value, which is 6.47 and 4.84 (in xx and yy directions, respectively) for PdPSeO, 5.98 and 5.78 for PdPSeS, and 6.44 and 6.05 PdPSeTe. The value for the zz direction is negligible as compared to these for the xx and yy directions. The plasma frequencies (the roots of the real part), according to the Drude model, appears at ~3.34 eV and 8.88 eV along the xx direction of the PdPSeO monolayer. In the case of PdPSeTe, the first frequencies are at the energy of 2.98 eV for xx and at 3.06 eV for yy direction, and the second frequencies appear at the energy of 8.79 eV for xx direction and 8.85 eV for yy direction (see Fig. 4(a)). All transitions from the valence bands to the conduction bands can be described by the imaginary components. The imaginary part increases at ~1.32 eV, 2.01 eV, and 1.70 eV for PdPSeO, PdPSeS and PdPSeTe, respectively (Fig. 4(b)), which are related to the corresponding bandgap values. The imaginary spectra increase from the bandgap to 3 eV for the PdPSeTe, to 4 eV for PdPSeO, and to 5 eV for PdPSeS monolayer. Obviously, the PdPSeTe and PdPSeO monolayers are strongly absorbing visible and ultraviolet light. The PdPSeTe monolayer can absorb the visible light more efficiently than the PdPSeO. Fig. 4(c) shows the absorption curves of the PdPSeX monolayers. The starting point of the increase appears at the same position of the corresponding value of the imaginary part. The absorption curves reveal the PdPSeTe monolayer has a larger efficiency to absorb light in the visible range than its counterparts. Fig. 4(d) illustrates the band alignments of the oxidation and reduction potentials for water splitting with respect to the band edges of PdPSeX monolayers.

The PdPSeS and PdPSeTe sheets have appropriate bandgap values ~2.02 eV, 1.70 eV, accordingly, and their band edges (conduction band edge (CBE) and valence band edge (VBE) are more negative and more positive, respectively, than the hydrogen reduction H^+/H_2 potential and the water oxidation H_2O/O_2 potential, respectively, for water splitting. The CBE is evaluated by $E_{CBE} = \chi - 0.5E_g - 4.5$ eV [59–61], then the VBE is estimated by $E_{VBE} = E_{CBE} + E_g$, where χ ($\chi = (\chi_{Pd}^2 \chi_P^2 \chi_{Se} \chi_X)^{1/6}$) eV is the geometric mean of electronegativity of the ingredient atoms and 4.5 eV is the free energy of the electron (with respect to the vacuum level). Herein, the E_{CBE} and E_{VBE} are the absolute values of the conduction and valence band edges, respectively. The E_{CBE} and E_{VBE} band edges are measured on the scale of the normal hydrogen electrode (NHE) potential of the reduction and oxidation levels of H_2O: the reduction level (H^+/H_2) is located at 0 eV, while the oxidation level (H_2O/O_2) at 1.23 eV. Therefore, the CBE should be located "above" the water reduction (H^+/H_2) level, and the VBE should be located "below" the water oxidation (H_2O/O_2) level, in the standard representation. Although the PdPSeO monolayer has a proper bandgap value, the position of the CBE makes it not applicable for water splitting/hydrogen production. Due to the adequate bandgap values and correct positions of the band edges of PdPSeS and PdPSeTe sheets, they are better candidates for water splitting than the PdPSe monolayer, and the best one in this regard is the PdPSeS.

5. Conclusion

The structural, mechanical, optical and electronic properties of the puckered penta-like PdPSeX (X=O, S, Te) Janus monolayers have been studied using the first-principles theory. Our results demonstrate that the structural parameters of PbPSeX monolayers depend strongly on the size of the X atom. The phonon spectra of the PbPSeX monolayers do not include negative frequencies confirming the monolayers' mechanically stability. The PbPSeX sheets are indirect semiconductors with bandgap values of 0.65 (1.44) eV, 1.20 (2.02) eV, and 0.98 (1.70) eV for PbPSeO, PbPSeS, and PbPSeTe monolayers according to the PBE (HSE06) functional. The optical properties examination indicates the PdPSeX monolayers have the ability to absorb the visible and ultraviolet range of spectrum. The PdPSeTe monolayer is revealed as the best candidate within this class of 2DMs for absorbing of visible light as well as for water splitting processes since it possesses the proper band alignment.

CRediT authorship contribution statement

A. Bafekry: Conceptualization, Methodology, Software, Writing – original draft, Formal analysis, Visualization, Investigation, Supervision, Project administration. **M. Faraji:** Methodology, Software, Investigation. **Mohamed M. Fadlallah:** Methodology, Software, Formal analysis, Writing – original draft. **H.R. Jappor:** Writing – review & editing. **N.N. Hieu:** Writing – review & editing. **M. Ghergherehchi:** Writing – review & editing. **D. Gogova:** Writing – review & editing.

Declaration of competing interest

The authors declare that they have no known competing financial interests or personal relationships that could have appeared to influence the work reported in this paper.

Acknowledgments

This work was supported by the National Research Foundation of Korea grant funded by the Korean government (NRF-2015M2B2A4033123). Computational resources were provided by TUBITAK ULAKBIM, at the High Performance and Grid Computing Center (TR-Grid e-Infrastructure).

Appendix A. Supplementary data

Supplementary material related to this article can be found online at https://doi.org/10.1016/j.apsusc.2021.152356.

References

[1] H. Li, Y. Shi, M.H. Chiu, L.J. Li, Emerging energy applications of two-dimensional layered transition metal dichalcogenides, Nano Energy 18 (2015) 293–305.
[2] A.O.M. Almayyali, B.B. Kadhim, H.R. Jappor, Stacking impact on the optical and electronic properties of two-dimensional $MoSe_2/PtS_2$ heterostructures formed by PtS_2 and $MoSe_2$ monolayers, Chem. Phys. 532 (2020) 110679.
[3] A. Bafekry, C. Stampfl, C. Nguyen, M. Ghergherehchi, B. Mortazavi, Tunable electronic properties of the dynamically stable layered mineral Pt_2HgSe_3 (Jacutingaite), Phys. Chem. Chem. Phys. 22 (2020) 24471–24479.
[4] A. Bafekry, C. Stampfl, M. Faraji, M. Yagmurcukardes, M.M. Fadlallah, H.R. Jappor, M. Ghergherehchi, S.A.H. Feghhi, A Dirac-semimetal two-dimensional BeN_4: Thickness-dependent electronic and optical properties, Appl. Phys. Lett. 20 (2021) 203103.
[5] A. Bafekry, M. Faraji, M.M. Fadlallah, I. Abdolhosseini Sarsari, H.R. Jappor, S. Fazeli, M. Ghergherehchi, Two-dimensional porous graphitic carbon nitride C_6N_7 monolayer: First-principles calculations, Appl. Phys. Lett. 119 (2021) 142102.
[6] A. Bafekry, M. Naseri, M.M. Fadlallah, I. Abdolhosseini Sarsari, M. Faraji, A. Bagheri Khatibani, M. Ghergherehchi, D. Gogova, A novel two-dimensional boron–carbon–nitride (BCN) monolayer: A first-principles insight, J. Appl. Phys. 130 (2021) 114301.
[7] X. Sun, S. Luan, H. Shen, S. Lei, Effect of metal doping on carbon monoxide adsorption on phosphorene: A first-principles study, Superlattices Microstruct. 124 (2018) 168–175.
[8] S. Deng, L. Li, Y. Zhang, Strain modulated electronic, mechanical, and optical properties of the monolayer PdS_2, $PdSe_2$, and $PtSe_2$ for tunable devices, ACS Appl. Nano Mater. 1 (2018) 1932–1939.
[9] S.-H. Zhang, B.-G. Liu, Hole-doping-induced half-metallic ferromagnetism in a highly-air-stable $PdSe_2$ monolayer under uniaxial stress, J. Mater. Chem. C. 6 (2018) 6792–6798.
[10] A.A. Puretzky, A.D. Oyedele, K. Xiao, A.V. Haglund, B.G. Sumpter, D. Mandrus, D.B. Geohegan, L. Liang, Anomalous interlayer vibrations in strongly coupled layered $PdSe_2$, 2D Mater. 5 (2018) 035016.
[11] A.N. Hoffman, Y. Gu, L. Liang, J.D. Fowlkes, K. Xiao, P.D. Rack, Exploring the air stability of $PdSe_2$ via electrical transport measurements and defect calculations, Npj 2D Mater. Appl. 2019 31 (3) (2019) 1–7.
[12] C. Soulard, X. Rocquefelte, P.-E. Petit, M. Evain, S. Jobic, J.-P. Itie, P. Munsch, H.-J. Koo, M.-H. Whangbo, Experimental and theoretical investigation on the relative stability of the PdS_2 - and pyrite-type structures of $PdSe_2$, Inorg. Chem. 43 (2004) 1943–1949.
[13] W. Lei, S. Zhang, G. Heymann, X. Tang, J. Wen, X. Zheng, G. Hu, X. Ming, A new 2D high-pressure phase of PdSe2 with high-mobility transport anisotropy for photovoltaic applications, J. Mater. Chem. C. 7 (2019) 2096–2105.
[14] E. Selb, M. Tribus, G. Heymann, Verbeekite, the long-unknown crystal structure of monoclinic $PdSe_2$, Inorg. Chem. 56 (2017) 5885–5891.

[15] X. Liu, H. Zhou, B. Yang, Y. Qu, M. Zhao, Strain-modulated electronic structure and infrared light adsorption in palladium diselenide monolayer, Sci. Rep. 7 (2017) 39995.

[16] A.D. Oyedele, S. Yang, L. Liang, A.A. Puretzky, K. Wang, J. Zhang, P. Yu, P.R. Pudasaini, A.W. Ghosh, Z. Liu, C.M. Rouleau, B.G. Sumpter, M.F. Chisholm, W. Zhou, P.D. Rack, D.B. Geohegan, K. Xiao, $PdSe_2$: Pentagonal two-dimensional layers with high air stability for electronics, J. Am. Chem. Soc. 139 (2017) 14090–14097.

[17] W.L. Chow, P. Yu, F. Liu, J. Hong, X. Wang, Q. Zeng, C.-H. Hsu, C. Zhu, J. Zhou, X. Wang, J. Xia, J. Yan, Y. Chen, D. Wu, T. Yu, Z. Shen, H. Lin, C. Jin, B.K. Tay, Z. Liu, High mobility 2D palladium diselenide field-effect transistors with tunable ambipolar characteristics, Adv. Mater. 29 (2017) 1602969.

[18] D. Qin, P. Yan, G. Ding, X. Ge, H. Song, G. Gao, Monolayer $PdSe_2$: A promising two-dimensional thermoelectric material, Sci. Rep. 81 (2018) 1–8.

[19] Y. Gao, X. Liu, W. Hu, J. Yang, Tunable n-type and p-type doping of two-dimensional layered $PdSe_2$ via organic molecular adsorption, Phys. Chem. Chem. Phys. 22 (2020) 12973–12979.

[20] Y. Shao, M. Shao, Y. Kawazoe, X. Shi, H. Pan, Exploring new two-dimensional monolayers: pentagonal transition metal borides/carbides (penta-TMB/Cs), J. Mater. Chem. A. 6 (2018) 10226–10232.

[21] Y. Wang, Y. Li, Z. Chen, Not your familiar two dimensional transition metal disulfide: structural and electronic properties of the PdS_2 monolayer, J. Mater. Chem. C. 3 (2015) 9603–9608.

[22] J. Xiao, M. Long, C.-S. Deng, J. He, L.-L. Cui, H. Xu, Electronic structures and carrier mobilities of blue phosphorus nanoribbons and nanotubes: A first-principles study, J. Phys. Chem. C. 120 (2016) 4638–4646.

[23] S. Zhang, J. Zhou, Q. Wang, X. Chen, Y. Kawazoe, P. Jena, Penta-graphene: A new carbon allotrope, Proc. Natl. Acad. Sci. USA 112 (2015) 2372–2377.

[24] Y. Ding, Y. Wang, Hydrogen-induced stabilization and tunable electronic structures of penta-silicene: A computational study, J. Mater. Chem. C. 3 (2015) 11341–11348.

[25] A. Lopez-Bezanilla, P.B. Littlewood, $\sigma - \pi$-Band inversion in a novel two-dimensional material, J. Phys. Chem. C. 119 (2015) 19469–19474.

[26] F. Li, K. Tu, H. Zhang, Z. Chen, Flexible structural and electronic properties of a pentagonal B_2C monolayer via external strain: A computational investigation, Phys. Chem. Chem. Phys. 17 (2015) 24151–24156.

[27] S. Liu, B. Liu, X. Shi, J. Lv, S. Niu, M. Yao, Q. Li, R. Liu, T. Cui, B. Liu, Two-dimensional penta-BP_5 sheets: High-stability, strain-tunable electronic structure and excellent mechanical properties, Sci. Rep. 7 (2017) 2404.

[28] M. Naseri, Arsenic carbide monolayer: First principles prediction, Appl. Surf. Sci. 423 (2017) 566–570.

[29] J.K. Burdett, B.A. Coddens, Geometrical-electronic relationships in the series palladium diphosphide, palladium phosphide sulfide, and palladium disulfide, Inorg. Chem. 27 (2002) 418–421.

[30] A. Hamidani, B. Bennecer, Electronic and optical properties of the orthorhombic compounds PdPX (X=S and Se), Comput. Mater. Sci. 48 (2010) 115–123.

[31] J.C.W. Folmer, J.A. Turner, B.A. Parkinson, Photoelectrochemical characterization of several semiconducting compounds of palladium with sulfur and/or phosphorus, J. Solid State Chem. 68 (1987) 28–37.

[32] J.V. Marzik, R. Kershaw, K. Dwight, A. Wold, Preparation and properties of PdPSe single crystals, J. Solid State Chem. 44 (1982) 382–387.

[33] T.A. Bither, P.C. Donohue, H.S. Young, Palladium and platinum phosphochalcogenides-synthesis and properties, J. Solid State Chem. 3 (1971) 300–307.

[34] W. Jeitschko, The structure of PdPS and the crystal chemistry of late transition-metal dipnictides and dichalcogenides, Acta Crystallogr. Sect. B. 30 (1974) 2565–2572.

[35] Y. Jing, Y. Ma, Y. Wang, Y. Li, T. Heine, Ultrathin layers of PdPX (X=S, Se): Two dimensional semiconductors for photocatalytic water splitting, Chem. - A Eur. J. 23 (2017) 13612–13616.

[36] P. Li, J. Zhang, C. Zhu, W. Shen, C. Hu, W. Fu, L. Yan, L. Zhou, L. Zheng, H. Lei, Z. Liu, W. Zhao, P. Gao, P. Yu, G. Yang, Penta-PdPSe: A new 2D pentagonal material with highly in-plane optical, electronic, and optoelectronic anisotropy, Adv. Mater. (2021) 2102541.

[37] A. Bafekry, M.M. Fadlallah, M. Faraji, A. Shafique, H.R. Jappor, I. Abdolhoseini Sarsari, Y.S. Ang, M. Ghergherehchi, Two-dimensional pentagonal material penta-pdpse: a first-principle study, arXiv:2109.04006v2 (2021).

[38] W. Chen, Y. Qu, L. Yao, X. Hou, X. Shi, H. Pan, Electronic, magnetic, catalytic, and electrochemical properties of two-dimensional janus transition metal chalcogenides, J. Mater. Chem. A 6 (2018) 8021–8029.

[39] X. Yang, D. Singh, Z. Xu, Z. Wang, R. Ahuja, An emerging janus MoSeTe material for potential applications in optoelectronic devices, J. Mater. Chem. C. 7 (2019) 12312–12320.

[40] A. Kandemir, H. Sahin, Bilayers of janus WSSe: monitoring the stacking type via the vibrational spectrum., Phys. Chem. Chem. Phys. 20 (2018) 17380–17386.

[41] A. Bafekry, S. Karbasizadeh, C. Stampfl, M. Faraji, D.M. Hoat, I.A. Sarsari, S.A.H. Feghhi, M. Ghergherehchi, Two-dimensional janus semiconductor BiTeCl and BiTeBr monolayers: a first-principles study on their tunable electronic properties via an electric field and mechanical strain, Phys. Chem. Chem. Phys. 23 (2021) 15216–15223.

[42] H.D. Bui, H.R. Jappor, N.N. Hieu, Tunable optical and electronic properties of janus monolayers Ga_2SSe, Ga_2STe, and Ga2SeTe as promising candidates for ultraviolet photodetectors applications, Superlattices Microstruct. 125 (2019) 1–7.

[43] A. Bafekry, M. Faraji, M.M. Fadlallah, H.R. Jappor, N.N. Hieu, M. Ghergherehchi, S.A.H. Feghhi, D. Gogova, Prediction of two dimensional bismuth-based chalcogenides Bi_2X_3 (X=S, Se, Te) monolayers with orthorhombic structure: A first-principles study, J. Phys. D: Appl. Phys. 54 (2021) 395103.

[44] A. Bafekry, I. Abdolhosseini Sarsari, M. Faraji, M.M. Fadlallah, H.R. Jappor, S. Karbasizadeh, V. Nguyen, M. Ghergherehchi, Electronic and magnetic properties of two-dimensional of FeX (X=S, Se, Te) monolayers crystallize in the orthorhombic structures, Appl. Phys. Lett. 118 (2021) 143102.

[45] A. Bafekry, M. Faraji, M.M. Fadlallah, H.R. Jappor, S. Karbasizadeh, M. Ghergherehchi, I.A. Sarsari, A.A. Ziabari, Novel two-dimensional of AlSb and InSb monolayers with double-layer honeycomb structure: A first-principle study, Phys. Chem. Chem. Phys. 23 (2021) 18752–18759.

[46] D.D. Vo, T.V. Vu, S. Al-Qaisi, H.D. Tong, T.S. Le, C.V. Nguyen, H.V. Phuc, H.L. Luong, H.R. Jappor, M.M. Obeid, N.N. Hieu, Janus monolayer PtSSe under external electric field and strain: A first principles study on electronic structure and optical properties, Superlattices Microstruct. 147 (2020) 106683.

[47] A. Bafekry, M. Faraji, S. Karbasizadeh, I. Abdolhosseini Sarsari, H.R. Jappor, M. Ghergherehchi, D. Gogova, Two-dimensional $FeTe_2$ and predicted janus FeXS (X: Te and Se) monolayers with intrinsic half-metallic character: tunable electronic and magnetic properties via strain and electric field, Phys. Chem. Chem. Phys. 23 (2021) 24336–24343.

[48] A. Bafekry, M. Yagmurcukardes, B. Akgenc, M. Ghergherehchi, C.V. Nguyen, Van der Waals heterostructures of MoS_2 and janus MoSSe monolayers on graphitic boron-carbon-nitride (BC_3, C_3N, C_3N_4 and C_4N_3) nanosheets: A first-principles study, J. Phys. D. Appl. Phys. 53 (2020) 355106.

[49] A. Bafekry, B. Mortazavi, M. Faraji, M. Shahrokhi, A. Shafique, H.R. Jappor, C. Nguyen, M. Ghergherehchi, S.A.H. Feghhi, Ab initio prediction of semiconductivity in a novel two-dimensional Sb_2X_3 (X=S, Se, Te) monolayers with orthorhombic structure, Sci. Rep. 11 (2021) 1–10.

[50] G. Kresse, J. Hafner, Ab initio molecular dynamics for liquid metals, Phys. Rev. B 47 (1993) 558.

[51] G. Kresse, J. Hafner, Efficient iterative schemes for ab initio total-energy calculations using a plane-wave basis set, Phys. Rev. B 49 (1994) 14251.

[52] J.P. Perdew, K. Burke, M. Ernzerhof, Generalized gradient approximation made simple, Phys. Rev. Lett. 77 (1996) 3865.

[53] J.P. Perdew, K. Burke, M. Ernzerhof, Generalized gradient approximation made simple, Phys. Rev. Lett. 78 (1997) 1396.

[54] J. Heyd, G.E. Scuseria, M. Ernzerhof, Screened hybrid density functionals applied to solids, J. Chem. Phys. 118 (2003) 8207.

[55] H.J. Monkhorst, J.D. Pack, Special points for brillouin-zone integrations, Phys. Rev. B 13 (1976) 12.

[56] G. Henkelman, A. Arnaldsson, H. Jonsson, A fast and robust algorithm for bader decomposition of charge density, Comput. Mater. Sci. 36 (2006) 354.

[57] D. Alfe, PHON: A program to calculate phonons using the small displacement method, Comput. Phys. Comm. 180 (2009) 2622.

[58] F. Mouhat, F.-X. Coudert, Necessary and sufficient elastic stability conditions in various crystal systems, Phys. Rev. B 90 (2014) 224104.

[59] H. Yu, S. Ouyang, S. Yan, Z. Li, T. Yu, Z. Zou, Solgel hydrothermal synthesis of visible-light-driven Cr-doped $SrTiO_3$ for efficient hydrogen, J. Mater. Chem. 21 (2011) 11347.

[60] M.M. Fadlallah, U. Eckern, Cation mono- and Co-doped anatase TiO_2 nanotubes: An ab initio investigation of electronic and optical properties, Phys. Status Solidi (B) 257 (2020) 1900217.

[61] A.A. Maarouf, D. Gogova, M.M. Fadlallah, Metal-doped $KNbO_3$ for visible light photocatalytic water splitting: A first principles investigation, Appl. Phys. Lett. 119 (2021) 063901.